Original Article

Aqueous humor proteomic analysis of acute angle-closure glaucoma with visual field loss

Jiyu Xu[1#^], Liangliang Zhao[2#], Xiang Liu[1,3], Haidan Sun[1], Xiaoyan Liu[1], Zhengguang Guo[1], Ying Wang[2], Wei Sun[1]

[1]Core Facility of Instrument, Chinese Academy of Medical Sciences, School of Basic Medicine, Peking Union Medical College, Beijing, China; [2]Department of Ophthalmology, The Second Hospital of Jilin University, Changchun, China; [3]Shanghai AB Sciex Analytical Instrument Trading Co., Ltd Beijing Branch Company, Beijing, China

Contributions: (I) Conception and design: J Xu, L Zhao; (II) Administrative support: W Sun, Y Wang; (III) Provision of study materials or patients: Y Wang, L Zhao; (IV) Collection and assembly of data: All authors; (V) Data analysis and interpretation: J Xu, W Sun; (VI) Manuscript writing: All authors; (VII) Final approval of manuscript: All authors.

[#]These authors contributed equally to this work.

Correspondence to: Wei Sun. Core Facility of Instrument, Chinese Academy of Medical Sciences, School of Basic Medicine, Peking Union Medical College, 5 Dong Dan San Tiao, Beijing 100005, China. Email: sunwei@ibms.pumc.edu.cn; Ying Wang. Department of Ophthalmology, The Second Hospital of Jilin University, 218 Ziqiang Street, Changchun 130041, China. Email: wangying9201@163.com.

Background: Acute angle-closure glaucoma (AACG) is an ophthalmic emergency that occurs over the course of hours or days and may cause irreversible blindness if not treated immediately. In most cases, optic nerve damage is the cause of visual field (VF) loss in AACG. There has been no reliable biomarker found to evaluate optic nerve damage to date. Aqueous humor (AH) proteome analysis might reveal the proteomic alterations in AACG and provide helpful clues in the search for an AH biomarker of optic nerve damage and VF loss.

Methods: In this study, we used the AH proteome to explore the functions of differentially expressed proteins (DEPs) during disease progression. The AH proteins from the early-stage group and late-stage group were extracted and analyzed by the data-independent acquisition (DIA) method. The DEPs functions were annotated, and parallel reaction monitoring (PRM) was used to validate the key DEPs.

Results: A total of 87 DEPs were found. Gene Ontology analysis showed that most DEPs were enriched in immunology, hemodynamics, and apoptosis. Ingenuity pathway analysis found that vascular endothelial growth factor (VEGF) signaling, the production of reactive oxygen species (ROS) in macrophages, and the nuclear factor erythroid 2-related factor 2 (NRF2)-mediated oxidative stress response were active pathways in the late stage of AACG. The mechanism of retinal ganglion cell (RGC) death was hypothesized on the basis of DEP functional analysis. A total of 20 DEPs were validated by using PRM, and prostaglandin-H2 D-isomerase was found to have the potential to evaluate optic nerve damage.

Conclusions: This study showed that AH proteomic analysis could reveal the proteomic alterations in the pathogenesis of VF loss in AACG and help to provide objective protein biomarkers to evaluate VF loss. These findings will benefit the application of the AH proteome to clinical research.

Keywords: Aqueous humor (AH); proteome; acute angle-closure glaucoma (AACG); visual field (VF) loss

Submitted Jan 29, 2021. Accepted for publication Sep 03, 2021.
doi: 10.21037/atm-21-457
View this article at: https://dx.doi.org/10.21037/atm-21-457

^ ORCID: 0000-0001-8505-5104.

Introduction

Glaucoma is a progressive optic neuropathy resulting in retinal ganglion cell (RGC) loss, optic nerve atrophy, and visual field (VF) loss (1). Acute angle-closure glaucoma (AACG) is an ophthalmologic emergency characterized by a rapid increase in intraocular pressure (IOP) due to an impaired outflow of aqueous humor (AH) (2). The incidence of AACG is usually higher among Asian populations (3). Reduced drainage leads to raised IOP, which potentially causes damage to the optic nerve (4). Despite adequate treatment, 3–12% of patients with acute angle closure develop long-term severe visual impairment, mainly as a result of glaucomatous optic neuropathy (4). Moreover, VF loss is not obvious under high IOP during acute AACG, and it progressively develops following acute AACG (3,5). Glaucomatous optic nerve damage occurs due to RGC death (6). To date, many studies have pointed out that ocular hemodynamic changes and vascular pathological changes tend to cause optic nerve ischemic reperfusion injury, eventually resulting in RGC death (7,8). Some molecules injure RGCs in various ways, one being nitric oxide (NO), which induces apoptosis and aggravates retinal damage. A high level of glutamate is also closely related to RGC death (9-11); however, a deep understanding of the RGC death mechanism in response to glaucoma is still lacking. Glaucoma patients can progressively and slowly develop optic nerve damage, even when IOP is well controlled (12). Biomarkers reflecting optic nerve damage could be of high clinical value. Optic nerve damage secondary to angle-closure leads to vision loss, and it has been traditionally determined by light microscopic evaluation of optic nerve cross sections (12). Currently, no reliable biomarkers have been found to evaluate optic nerve damage. Therefore, an improved molecular investigation may illustrate the relative changes in AACG and offer evidence for screening biomarkers.

The AH is an integral component in many ocular health functions, including nutrient and oxygen supply, removal of metabolic waste, ocular immunity, and ocular shape and refraction (13). The major constituents of AH are proteins (including proteins derived from the protein exchanges across the AH, vitreous fluid, retina, and optic nerve head), water, and electrolytes (14,15). Although proteins in AH are present in relatively low concentrations compared to blood serum, they are vital for the maintenance of anterior segment homeostasis (15). Proteins secreted from anterior segment tissues play a role in various eye diseases, such as oedema, neovascularization, cataracts, and glaucoma (16-19). In glaucoma, elevated IOP causes damage to the optic nerve head (20), which may then release related components to reflect vitreous fluid (21); these then might be detected in AH via the vitreous–aqueous exchange. In this way, it may be possible to locate optic nerve damage biomarkers in the AH proteome. Technological advancements have allowed for high-throughput proteomic studies that examine biofluids such as AH, vitreous humor, tears, and serum (15). A better understanding of the AH proteomic changes that occur during the development of eye diseases may provide clues in the search for AH biomarkers.

Previous studies have suggested that the AH proteome could reflect alterations in glaucomatous eyes. As early as 2010, Izzotti *et al.* reported AH proteome alterations in primary open-angle glaucoma (22). In 2016, Kliuchnikova *et al.* investigated 29 human AH samples from cataract and glaucoma patients with and without pseudoexfoliation syndrome. They identified 215 proteins in AH from glaucoma samples using high-resolution liquid chromatography with tandem mass spectrometry (LC-MS/MS) and found that AH proteins could reflect the neural origin of the eye; decreased apolipoprotein D was also defined as a marker of pseudoexfoliation syndrome (16). Kaeslin *et al.* defined 87 proteins that were differentially expressed between glaucomatous and control AH, and the differentially expressed proteins (DEPs) were found to be involved in cholesterol-related, inflammatory, metabolic, antioxidant, and proteolysis-related processes (23). In 2019, Wang *et al.* analyzed the differential expression of AH proteins between acute primary angle-closure glaucoma (APACG) combined with cataracts and cataracts alone and found that the change in proteins in AH was related to the APACG (24). Previous studies have shown that the AH proteome could reflect proteomic changes in glaucoma and provide potential AH biomarkers. To our knowledge, AH proteome studies of VF loss in glaucoma are still unavailable. Therefore, in this study, we investigated the functions of AH proteins in VF loss in glaucoma by applying a proteomic strategy, with the greater aim of identifying biomarkers to assess optic nerve damage from AH proteins.

We obtained AH samples from early- and late-stage patients. The data-independent acquisition (DIA) method was performed to define the DEPs. The functions of the DEPs were annotated by Gene Ontology (GO) and ingenuity pathway analysis (IPA). Furthermore, parallel

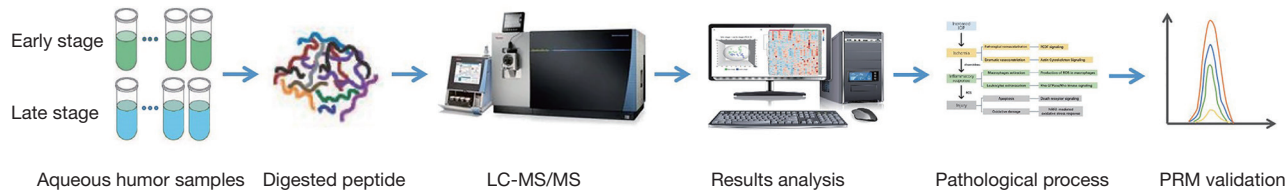

Figure 1 The workflow of this study. Permission was obtained from Thermo Fisher Scientific to use the image of Orbitrap Fusion Lumos Tribrid Mass Spectrometry. LC-MS/MS, liquid chromatography-tandem mass spectrometry; PRM, parallel reaction monitoring.

Table 1 The clinical information of the two cohorts

Characteristics	Experimental group		Validation group	
	Late stage	Early stage	Late stage	Early stage
Gender (F/M)	14/2	13/2	10/1	9/1
Age (year)	68.88	66.2	69.36	61.20[a]
VFI	14.10	93.53[b]	5.27	91.60[b]
IOP (mmHg)	28.77	20.17	24.67	29.33

[a], P<0.05 for 2 stages; [b], P<0.001 for 2 stages. VFI, visual field index; IOP, intraocular pressure.

reaction monitoring (PRM) was used to validate the key AH proteins. The goal of this study was to investigate the proteomic alterations in AACG and provide helpful clues for finding potential VF loss biomarkers in AH proteins. (*Figure 1*).

We present the following article in accordance with the MDAR reporting checklist (available at https://dx.doi.org/10.21037/atm-21-457).

Methods

Ethical approval

All volunteers were given a verbal explanation of the study before enrolment, and each participant signed an informed consent form. The consent procedure and the research protocol for this study were approved by the Ethics Committee for Human and Animal Research in Peking Union Medical College (No. 047-2019). The study methodologies conformed to the Declaration of Helsinki (as revised in 2013).

Clinical information

In this study, a total of 52 individuals were included and divided into 2 cohorts according to their visual field index (VFI). The late-stage (LS) cohort included 27 AACG patients with a VFI lower than 50, and the early-stage (ES) cohort included 25 AACG patients with a VFI higher than 80, according to the glaucoma staging system (25), where VFI >80 indicates early stage, and VFI <50 indicates severe and end stage. The clinical information of the 2 cohorts is shown in *Table 1* and Table S1. All AACG patients were on anti-\glaucoma medication with the same drugs (topical alpha receptor agonists, topical carbonic anhydrase inhibitors, topical beta-blockers, and systemic carbonic anhydrase inhibitors), and no patients had cataracts. The IOP was measured before glaucoma surgery, and there was no statistical difference between the 2 groups. The VFI data were also collected before surgery. The mean ages of all participants ranged from 60 to 70 years, and the age-related difference was not remarkable.

Reagents and instruments

Ammonium bicarbonate, dithiothreitol (DTT), formic acid, high-performance liquid chromatography (HPLC)-grade acetonitrile (ACN), iodoacetamide (IAM), and trifluoroacetic acid were purchased from Sigma-Aldrich (St. Louis, MO, USA). Sequencing-grade trypsin was purchased from Promega (Madison, WI, USA).

An Orbitrap Fusion Lumos Tribrid Mass Spectrometer coupled with an EASY-nLC 1000 (Thermo Fisher Scientific, Bremen, Germany) was employed in the discovery phase.

A Triple TOF 5600 mass spectrometer (AB Sciex, Framingham, MA, USA) coupled with an ACQUITY UPLC system (Waters Corp., Milford, MA, USA) was used in the validation phase.

Clinical materials

All participants underwent an ophthalmic evaluation, including IOP measurement, VFI value measurement, best

corrected visual acuity (BCVA) measurement, gonioscopy testing, and fundus examination. The inclusion criteria for AACG were as follows: most of the angle was closed, IOP was increased, and fundus changes and VF defects could be found in the glaucoma optic nerve injury. Patients with autoimmune diseases, malignant tumors, severe liver disease, and previous ocular surgery were excluded. The AH samples were obtained from glaucoma patients during surgery. Each sample was approximately 50–200 μL and was aspirated from the anterior chamber using a 26-gauge needle before the start of surgery. A total of 52 AH samples were collected. These samples were randomly divided into 2 groups: the experimental group (31 samples: 15 from early stage and 16 from late stage) and the validation group (21 samples: 10 from the early stage and 11 from the late stage). After collection, the AH samples were immediately centrifuged at 2,500 ×g for 10 minutes at 4 ℃ to remove the cellular components (CC) and debris, and the supernatants were stored at –80 ℃ until further analysis.

Protein extraction and digestion

From each AH sample, 5 μL was taken for a pooled sample. The pooled sample was used as quality control (QC) sample, which was injected frequently to monitor the reproducibility of the LC-MS/MS. The AH samples and the pooled sample were precipitated overnight using 3 times the volume of ethanol at 4 ℃. Then, the pellets were centrifuged at 10,000 ×g for 30 minutes and resuspended in lysis buffer (7 M urea, 2 M thiourea, 0.1 M of DTT, and 5 mM of Tris; pH =8). The protein concentrations of AH samples were determined by spectrophotometry based on the Bradford method.

The filter-aided sample preparation (FASP) method was used for protein digestion with trypsin. The protein samples (200 μg) were deoxidized with 20 mM DTT for 5 min at 95 ℃ and carbamidomethylated with 50 mM IAM for 45 min at room temperature in the dark. Then, the samples were digested with trypsin (4 μg) in 25 mM of NH_4HCO_3 buffer (pH =8) and incubated at 37 ℃ overnight. After digestion, the peptides were desalted with a C18 solid-phase extraction column (Waters Oasis, Dublin, Ireland), washed with 500 μL of 0.1% formic acid, eluted with 500 μL of 100% ACN, and then vacuum-dried.

Offline HPLC

The lyophilized peptide mixture was redissolved in 0.1% formic acid, and a high-pH reversed-phase liquid chromatography (RPLC) column from Waters (4.6 mm × 250 mm, Xbridge C18, 3 μm) was used for fractionation. The peptide mixture was loaded onto the column in buffer A2 (H_2O, pH =10). The elution gradient, 5–30% buffer B2 (90% ACN; pH =10; flow rate, 1 mL/min), was applied for 60 minutes. The eluted peptides were collected at 1 fraction per minute, and a total of 60 fractions were collected from 1 to 60. The 60 fractions were then vacuum-dried, resuspended in 0.1% formic acid, and pooled into 20 samples by combining fractions 1, 21, and 41; 2, 22, and 42; and so on.

Liquid chromatography with tandem mass spectrometry

Orbitrap Fusion Lumos Tribrid (Thermo Scientific) coupled with the EASY-nLC 1000 was used for analysis in the data-dependent acquisition-mass spectrometry (DDA-MS) and DIA-MS modes. The digested peptides were separated on an RP C18 self-packing capillary LC column (75 μm ×100 mm; particle size 3 μm). The eluted gradient was 5–30% buffer B2 (0.1% formic acid, 99.9% ACN; flow rate, 0.3 μL/min), and peptides were eluted for 60 minutes.

To generate a spectral library, the 20 HPLC samples were analyzed in DDA mode. The parameters included the use of positive-mode and data-dependent MS/MS scans being performed per full scan with the top-speed mode (3 s). Precursor spectra (350–1,500 m/z) were collected with a resolution of 60,000, and the automatic gain control (AGC) target was set to 1e6. Fragment spectra were collected at a resolution of 15,000. The isolation width was set to 1.6 Da with a collision energy of 32%. Only precursors charged between +2 and +5 were acquired. Dynamic exclusion had a duration of 30 s, and the maximum injection time was 50 ms.

For DIA analysis, a variable isolation window with 38 windows was employed for MS acquisition. The specific window lists were constructed based on the DDA experiment of the pooled sample. According to the precursor m/z distribution of the pooled sample, the precursor ion number was equalized in each isolation window. The full scan range was set from 400 to 900 m/z and screened at a resolution of 120,000, followed by DIA scans with a resolution of 30,000 (higher-energy C-trap dissociation [HCD] collision energy: 32%; AGC target: 1e6; maximum injection time: 50 ms).

PRM analysis

A Triple TOF 5600 mass spectrometer (AB Sciex,

Framingham, MA, USA) was used for PRM analysis. An RP C18 self-packing capillary LC column (75 μm ×100 mm, 3 μm) was used to separate the peptides. The eluted gradient was 5–30% buffer B1 (0.1% formic acid, 99.9% ACN; flow rate, 0.3 μL/min), and peptides were eluted for 60 minutes. A spray voltage of 2.10 kV and a capillary temperature of 60 ℃ were used for ionization. The peptides (Table S2) were monitored by PRM acquisition mode to perform MS/MS scans of the precursor ions for all peptide markers along the complete chromatographic run, and each sample was run twice. The normalized collision energy was fixed to 35%, and the accumulated time was 300 s.

Data processing

The DDA data were then processed and analyzed by Proteome Discoverer (Thermo Scientific) software and searched against the human SwissProt database appended with the indexed retention time (iRT) fusion protein sequence (Biognosys, Zurich, Switzerland). The search was set as follows: up to 2 missed cleavage sites were included, carbamidomethyl cysteine was set as a fixed modification, and the precursor and fragment ion mass tolerances were 10 ppm and 0.02 Da, respectively. The applied false discovery rate (FDR) for protein identification was less than 1.0%. The results were imported to Spectronaut Pulsar (Biognosys) software to generate a spectral library.

The raw DIA data were analyzed by Spectronaut Pulsar (Biognosys) with default settings. In brief, the retention time prediction type was set to dynamic iRT. Interference correction on the MS2 level was enabled. Peptide intensity was calculated by summing the peak areas of their respective fragment ions for MS2, and the protein intensity was calculated by summing the intensity of their respective peptides. Cross-run normalization was enabled to correct for systematic variance in the LC-MS/MS performance, and a local normalization strategy was used. The normalization was based on the assumption that on average, a similar number of peptides was upregulated and downregulated, and the majority of the peptides within the sample were not regulated across runs or during the retention time (26). Protein inference was performed with the ID picker algorithm implemented in Spectronaut. All results were filtered by a Q value cutoff of 0.01 (corresponding to an FDR of 1%).

For the PRM mode, Skyline software (version 3.5.0.9319; https://skyline.ms/project/home/begin.view) was used for the selection of the suitable m/z precursor ion to m/z fragment ion transition for the selected candidate peptide biomarkers. Peptide settings were as follows: trypsin [KR/P] enzyme, up to 2 missed cleavage sites, a peptide length range from 8 to 25, 2 variable modifications of carbamidomethyl on Cys and oxidation on Met, and a maximum number of variable modifications of 3. Transition settings were as follows: the precursors were charged to 2 and 3; the ions were charged to 1 and 2; and the ion types were set as b, y, and p. The product ions were set to range from ion 3 to the last ion, and the ion match tolerance was set as 0.02 Da.

Statistical analysis

For DIA results, DEPs were defined as upregulated when abundance was ≥1.5-fold increase, or as downregulated when abundance was ≤0.67-fold reduced relative to early-stage group. For PRM results, the abundance change of peptides was inspected. In addition to a cutoff value of 1.5-fold change relative to the early stage group, an adjusted P value (Bonferroni method) <0.05 was applied to define differential peptides.

Bioinformatics analysis

For the GO analysis, all of the DEPs were analyzed using R software (package: ClusterProfiler; The R Foundation for Statistical Computing; https://bioconductor.org/packages/release/bioc/html/clusterProfiler.html).

For the IPA analysis, the SwissProt accession numbers were uploaded to IPA software (Ingenuity Systems, Mountain View, CA, USA). The proteins were mapped to the disease and functional categories, canonical pathways available in Ingenuity Knowledge Base, and other databases that were ranked by the P value.

Results

Differential proteomic analysis

In total, 31 patients were included in the experimental group, including 16 patients from the late stage and 15 patients from the early stage. The 31 AH samples were analyzed using DIA methods, and overall, a total of 519 proteins (including 503 proteins with at least 2 unique peptides) were identified, with an average of 402 proteins being detected in each sample (available online: https://cdn.amegroups.cn/static/public/atm-21-457-1.xlsx).

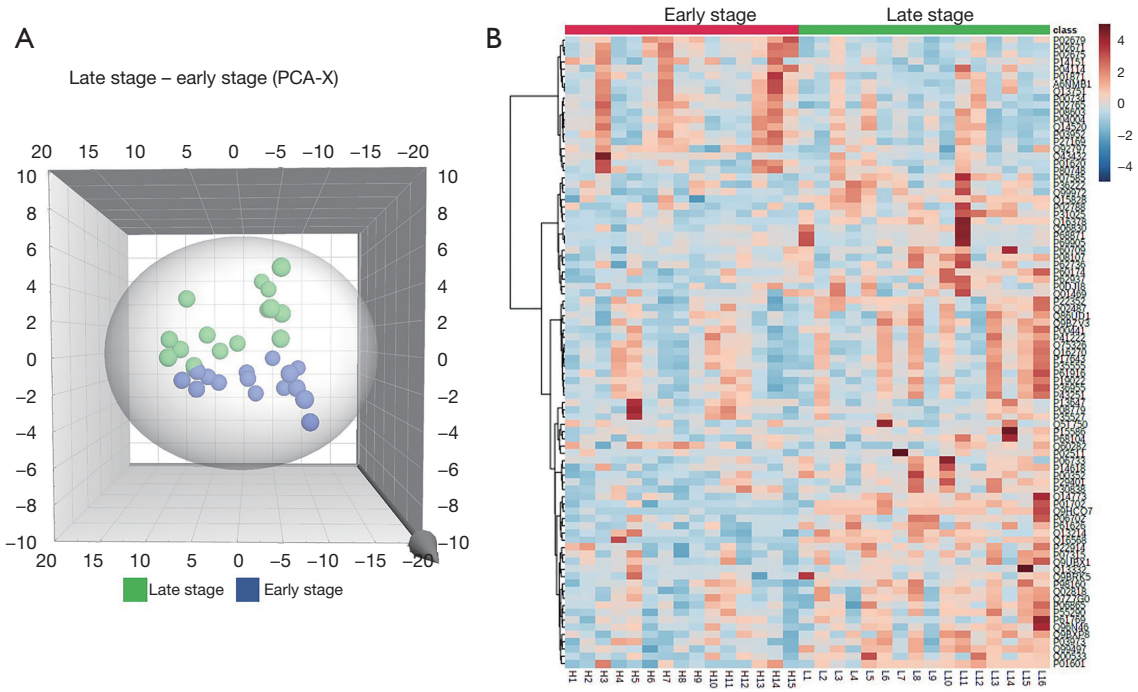

Figure 2 AH proteome profile analysis. (A) 3D plot of the PCA result. The ellipse represents a 95% confidence interval using Hotelling's T2 statistic. Observations situated far outside the ellipse are outliers. (B) Heatmap of 87 DEPs between the 2 groups. AH, aqueous humor; PCA, principal component analysis. DEPs, differentially expressed proteins.

The technical variation in the analysis was evaluated by calculating the coefficient of variation (CV) of the protein abundance among 4 QC replicates (R^2=0.864). As a result, 393 proteins with CV <0.6 were used to identify the DEPs (Figure S1).

To show the difference between the 2 groups, principal component analysis (PCA) was used. The 3D plot showed that the 2 groups had clear distinctions in their proteomics profiles (*Figure 2A*).

To identify the DEPs, the cutoff value of a 1.5-fold change (late stage/early stage) between the 2 groups was used. A total of 87 proteins were found, among which 23 were downregulated and 64 were upregulated. A heatmap based on the DEPs showed that the 2 groups expressed different proteomic patterns (*Figure 2B*).

Biological function analysis of the DEPs

To further investigate the biological function of the different proteins, 87 DEPs were subjected to GO annotations and IPA analysis.

The GO annotations for biological process (BP), CC, and molecular function (MF) were determined (ClusterProfiler, R software; *Figure 3A-3C*). In the BP category, GO terms relating to immunology, hemodynamics, and apoptosis were mostly enriched. In the CC category, collagen-containing extracellular matrix (ECM; P=3.54E-18, ratio =0.29) showed the highest percentage. Regarding the MF category, cell adhesion was overrepresented. The upregulated cell adhesion proteins in this study were related to cell–ECM adhesions, including fibrillin-1, vitronectin, and cadherin. According to a previous study, the RGC loss in glaucoma is associated with the ECM in the optic nerve head prelaminar region (27). In the prelaminar region of the optic nerve head, the connective tissue sheaths around the capillaries are thickened, which can influence the oxygen and nutrition transport, and finally contribute to RGC loss (28).

The IPA analysis revealed further detailed functional changes of the DEPs (*Figure 4A*, available online: https://cdn.amegroups.cn/static/public/atm-21-457-2.xls). In accordance with the GO annotations for BP, many of the proteins were relevant to vascular disease, cell death and survival, and the inflammatory response. Additionally, a few proteins were involved in neurological disease, which suggests that neurodegenerative processes occurred during the progression of symptoms (29). Notably, quantity of Ca^{2+}

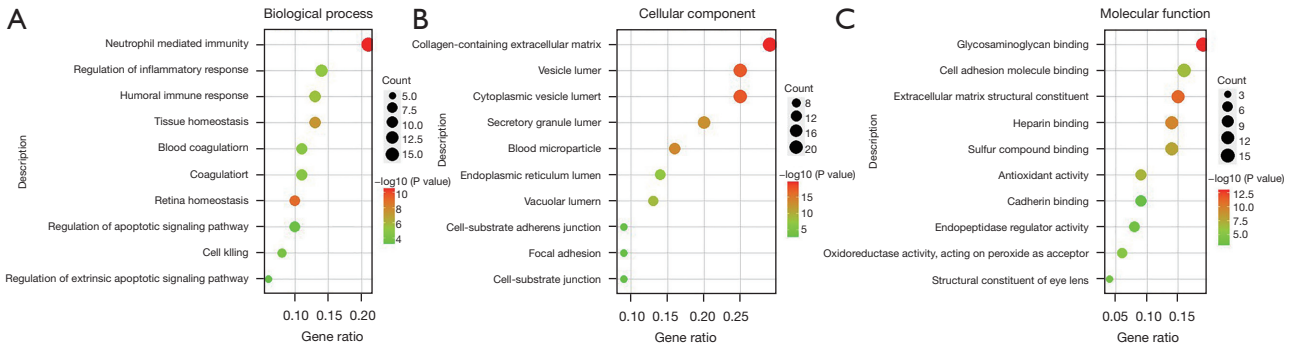

Figure 3 The GO annotations of DEPs. (A) Biological Process. (B) Cellular Component. (C) Molecular Function. GO, Gene Ontology; DEPs, differentially expressed proteins.

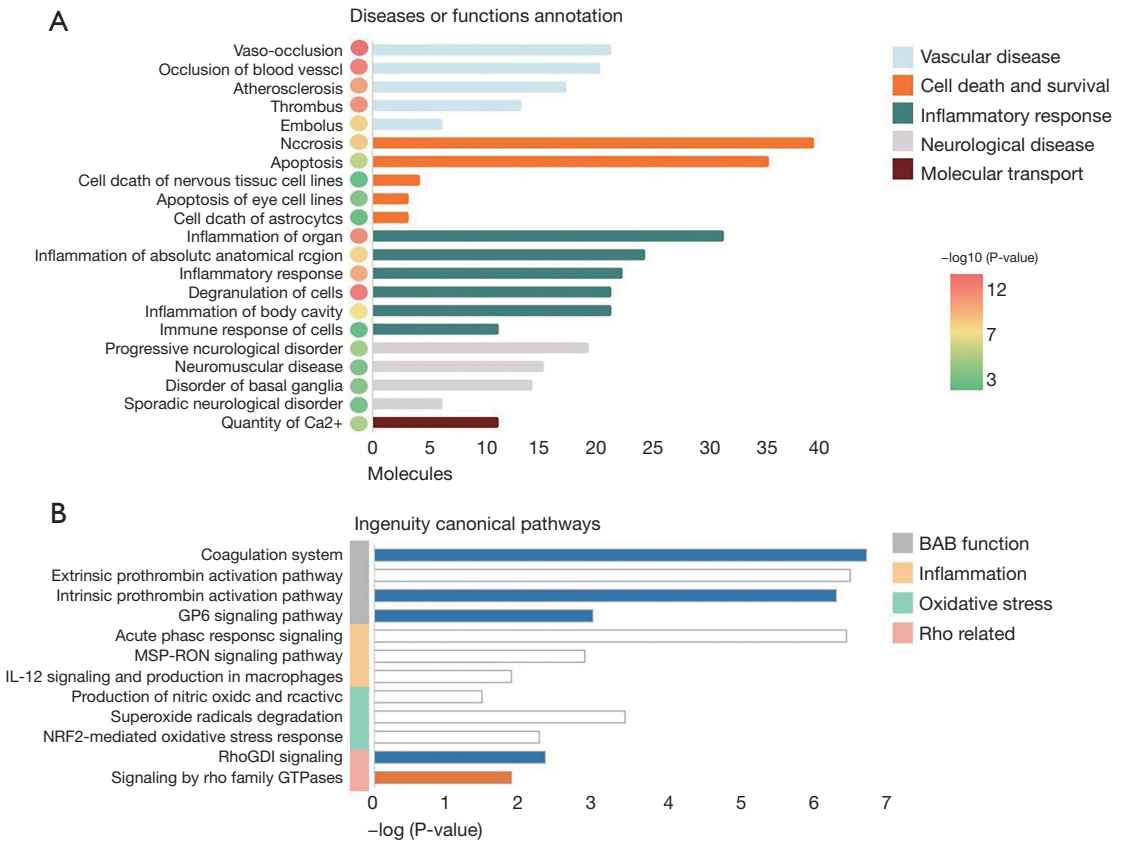

Figure 4 IPA analysis of DEPs. (A) The diseases or functions annotation. The color of the dot indicates the level of significance. (B) The major canonical pathways of DEPs. The orange bar represents significantly activated, the blue bar represents significantly inhibited, and the white bar represents no significant change. BAB, blood-aqueous humor barrier; IPA, ingenuity pathway analysis; DEPs, differentially expressed proteins.

Table 2 Validated proteins by parallel reaction monitoring

Accession	Protein name	Peptides	DIA fold change	PRM fold change	PRM P value	AUC
P41222	Prostaglandin-H2 D-isomerase	AQGFTEDTIVFLPQTDK	1.65	5.36	0.003	1.000
P61916	NPC intracellular cholesterol transporter 2	EVNVSPCPTQPCQLSK	1.51	4.50	0.003	0.991
P35555	Fibrillin-1	CECFPGLAVGLDGR ISPDLCGR	1.63	2.33	0.002	0.989
P36955	Pigment epithelium–derived factor	ELLDTVTAPQK TSLEDFYLDEER LQSLFDSPDFSK KTSLEDFYLDEER	1.55	3.08	0.001	0.988
Q86UD1	Out at first protein homolog	ALILGELEK	1.81	2.67	0.003	0.982
O75326	Semaphorin-7A	VYLFDFPEGK	1.56	2.62	0.004	0.964
P36222	Chitinase-3-like protein 1	EGDGSCFPDALDR	1.61	8.29	0.005	0.964
P08603	Complement factor H	CTSTGWIPAPR	0.65	0.29	0.005	0.927
P19022	Cadherin-2	ESAEVEEIVFPR	1.54	2.83	0.013	0.927
P07585	Decorin	DFEPSLGPVCPFR VVQCSDLGLDK	2.30	2.26	0.012	0.925
Q01469	Fatty acid-binding protein 5	TTQFSCTLGEK	2.09	3.62	0.001	0.909
Q13214	Semaphorin-3B	TCCYQALLVDEER	1.51	2.89	0.002	0.891
Q15828	Cystatin-M	VTGDHVDLTTCPLAAGAQQEK	1.84	2.49	0.015	0.891
P02765	Alpha-2-HS-glycoprotein	TVVQPSVGAAAGPVVPPCPGR	0.58	0.38	0.010	0.882
P04004	Vitronectin	DVWGIEGPIDAAFTR	0.64	0.52	0.007	0.864
P69905	Hemoglobin subunit alpha	LRVDPVNFK	19.66	1.96	0.028	0.864
P03973	Antileukoproteinase	CLDPVDTPNPTR	1.61	1.80	0.037	0.836
P02679	Fibrinogen gamma chain	VGPEADKYR	0.35	0.59	0.027	0.809
Q16568	Cocaine- and amphetamine-regulated transcript protein	YGQVPMCDAGEQCAVR	1.91	1.92	0.046	0.800
P61769	Beta-2 microglobulin	VNHVTLSQPK	1.89	2.52	0.046	0.755

DIA, data-independent acquisition; PRM, parallel reaction monitoring; AUC, area under curve.

function was annotated, which was associated with the death of inner retinal cells in a previous report (30).

The IPA analysis of canonical pathways indicated those pathways in which the DEPs were enriched (*Figure 4B*, available online: https://cdn.amegroups.cn/static/public/atm-21-457-2.xls). Pathways related to blood–aqueous barrier (BAB) function, inflammation, and oxidative stress were found, and Rho-related pathways were also observed.

PRM validation

To validate the results of the discovery phase, 21 samples were recruited, including 11 samples from the early-stage group and 10 from the late-stage group. Technical variation in the PRM analysis was evaluated by calculating the CV of the peptide abundance among 3 QC replicates (R^2=0.975), and the distribution of the CVs is shown in Figure S2. A

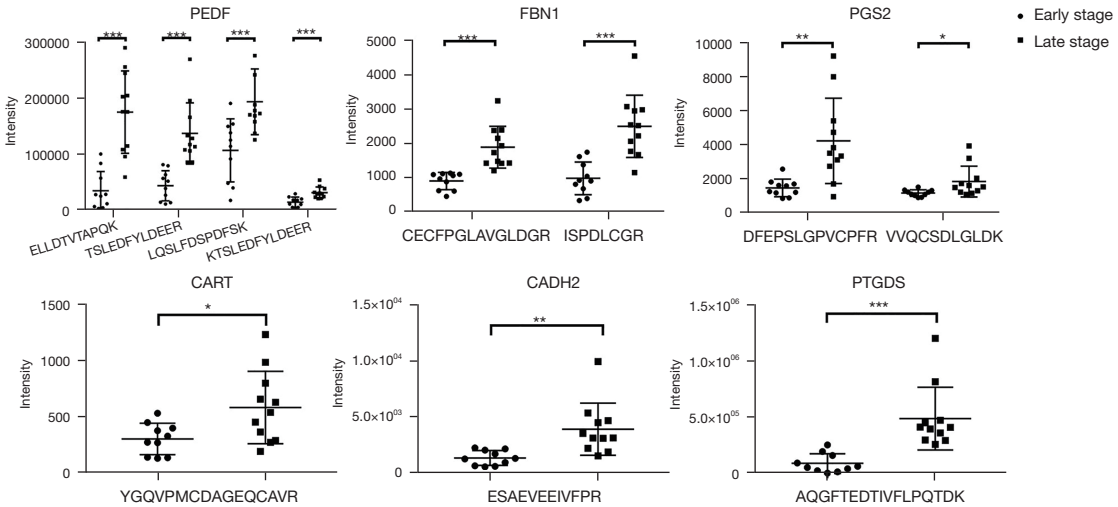

Figure 5 The validated proteins by PRM method. Peptides form the same protein are shown in a plot. Detailed information is shown in Table S2. The asterisks indicate the level of significance. *, P<0.05; **, P<0.01; ***, P<0.001. PRM, parallel reaction monitoring; PEDF, pigment epithelium-derived factor; FBN1, fibrillin-1; CART, cocaine- and amphetamine-regulated transcript; CDH2, cadherin-2; PTGDS, prostaglandin-H2 D-isomerase.

total of 20 proteins (16 upregulated and 4 downregulated) showed consistent results with the experimental group results (*Table 2*, Table S2). The abundance change of peptides was inspected (Figure S3). Among them, 4 peptides from PEDF, 2 peptides from FBN1, and 2 peptides from PGS2 were validated. The peptides of several key proteins (CART, CDH2, and PTGDS) were also validated, and peptides from the same protein showed a similar trend (*Figure 5*).

The performance of these proteins in distinguishing early-stage VF loss from late-stage VF loss was evaluated by receiver operating characteristic (ROC) analysis, and the results ranged from 0.755 to 1.000 (*Table 2*). Among them, prostaglandin-H2 D-isomerase (PTGDS) could achieve the best results (ROC =1) and might be clinically useful as an optic nerve damage biomarker.

Discussion

As previous studies have reported, the AH proteome correlates with the mechanisms of many eye disorders (31-33). In this study, we used the AH proteome to evaluate the characteristics of VF loss in the AACG cohort. A total of 87 DEPs were found. The DEPs functional analysis helped further clarify the pathological changes involved. In general, AACG-related processes were annotated in our study, especially those induced by ischemia, such as ocular hemodynamic and vascular changes, immune response, and apoptosis.

Regarding ocular hemodynamics, increased IOP can lead to hemodynamic changes in the ocular blood vessels that supply the optic nerve (7). Alterations may cause ischemic death of RGCs by reducing the supply of oxygen and nutrients (34,35). Additionally, blocked vessels and abnormal vascular walls result in dysfunction of the eye vessels, which may lead to poor perfusion in the eyes and ischemic injury (3). This study found many of the DEPs were involved in vascular pathological changes, such as vaso-occlusion and thrombus. These phenomena tended to cause ischemia in the eyes and then lead to injuries to the local tissue. Moreover, ischemia- and hypoxia-induced pathological ocular angiogenesis may lead to significant visual impairment (36). A previous study observed the development of tortuous and dilated retinal vessels throughout the whole retina in an ocular hypertension mouse model (5). These findings indicated the AACG might be related to ocular neovascularization (5). The role of ocular angiogenesis should be borne in mind when investigating the progression of optic neuropathy. Once angiogenesis occurs, the function of pigment epithelium-derived factor (PEDF) has to be determined, which has potent antiangiogenic actions and protective effects against retinal cell death (37). It was reported that PEDF overexpression ameliorated ischemia-induced retinal

neovascularization contributed to a protective effect on the blood-retinal barrier and attenuated pathological neovascularization under pathogenic conditions (37). In this study, we observed that the expression of PEDF was significantly different between the 2 groups. The upregulation of PEDF in the late-stage group might have promoted the regression of neovascularization by suppressing the angiogenic effects of hypoxia inducible factor-1 (HIF-1), decreasing vascular endothelial growth factor (VEGF) levels, and downregulating matrix metalloproteinases (MMP)-2 and -9 expression and activities (36).

Another protein-regulating vascular function that was identified in our study was cocaine- and amphetamine-regulated transcript (CART). A previous study revealed the mechanism by which CART regulates vascular tone (38): CART stimulates the de novo synthesis of bioactive endothelin and newly synthesized endothelin and then activates smooth muscle-bound ETA receptors, evoking dramatic vasoconstriction (38). A previous study reported that CART increased neuronal cell death in culture and was associated with higher mortality after experimental stroke *in vivo* (39). In the same study, researchers proposed that the vasoconstriction effect of CART is amplified in the ischemia-compromised cerebral circulation, exacerbating injury and hindering recovery from stroke (39). The results observed in this study showed an upregulation of CART in the late-stage group and that a high level of CART might constrict the blood vessels as mentioned above, reducing the blood flow, and then causing ischemic injury.

In glaucoma, inflammatory responses have been identified as common features, both in clinical and in experimental settings (29). Under normal conditions, AH exhibits anti-inflammatory potential, which inhibits neutrophil activation, suppresses NO production by macrophages, and interferes with complement activation (40). In this study, many DEP functions were related to inflammatory response, such as neutrophil-mediated immunity and NO production by macrophages, which may result in the death of RGCs and the loss of sight (41). A previous study pointed out that ischemic events could produce a large number of chemokines that attract leukocytes (42). A mass of leukocytes blocks blood vessels and breaks the blood-retina barrier (BRB), causing failed filtration of the leukocytes (42). Other studies reported that Rho GTPase/Rho kinase signaling contributes to leukocyte extravasation (43-45). In our study, this pathway was predicted as being more active in the late-stage group, indicating that leukocyte extravasation was more facilitative in the late-stage group. As a result, these immune cells would be distributed ubiquitously in the ischemic region and produce an abundance of reactive oxygen species (ROS) while performing their functions (46). It has been reported that ROS are cytotoxic to RGCs and to lead to necrotic cell death by direct oxidative damage to cellular constituents and apoptotic death (47-50). In this study, we found the NRF2 pathway in our pathway analysis and superoxide radical degradation-related proteins (SOD1 and TYRP1) were upregulated in the late-stage group, which may be a response to excessive ROS. Our results and previous studies (41,46) indicated that ocular ischemia might activate inflammation pathways and produce massive amounts of ROS, finally causing damage to RGCs.

The functional annotation by IPA showed that many DEPs were related to the process of cell death, including the death of nervous tissue cell lines, the death of astrocytes, and the apoptosis of eye cell lines. Apoptosis is the main pathogenesis after retinal ischemia-reperfusion (RIR) and causes injury to RGCs (51). A previous study found that excess Ca^{2+} and ROS can cause the activation of BH3-only proteins and then activate Bax, resulting in apoptosis (52). The IPA function analysis results showed quantity of Ca^{2+}, superoxide radicals degradation, and the death receptor signaling pathway were upregulated in the late group. Another apoptosis-related pathway, BEX2 was also found in the IPA analysis, and a previous study reported that BEX2 pathway downregulation promoted cell apoptosis (53); therefore, it might be a protective mechanism in glaucoma. In the BEX2 pathway, cadherin-2 (CDH2) has been previously demonstrated to decrease the apoptosis of mouse endothelial cells in culture (54). In this study, CDH2 was upregulated in the late-stage group, and thus might have a protective effect on RGCs and reduce apoptosis.

Taken together, we integrated the results of functional analysis and attempted to infer the connection between them. Other studies have reported that elevated IOP during AACG altered the function of blood vessels in the eye, causing ischemia, while other activities, such as neovascularization and vasoconstriction, also contributed to ischemia (3,7,34,35). Focal ischemia might induce an inflammatory response, and then immune cells might produce harmful ROS. Eventually, excessive ROS results in apoptosis by activating the apoptotic pathway and causing oxidative damage to the cells (*Figure 6*).

We also sought to use AH protein biomarkers to provide an objective evaluation of VF loss. Among the 20

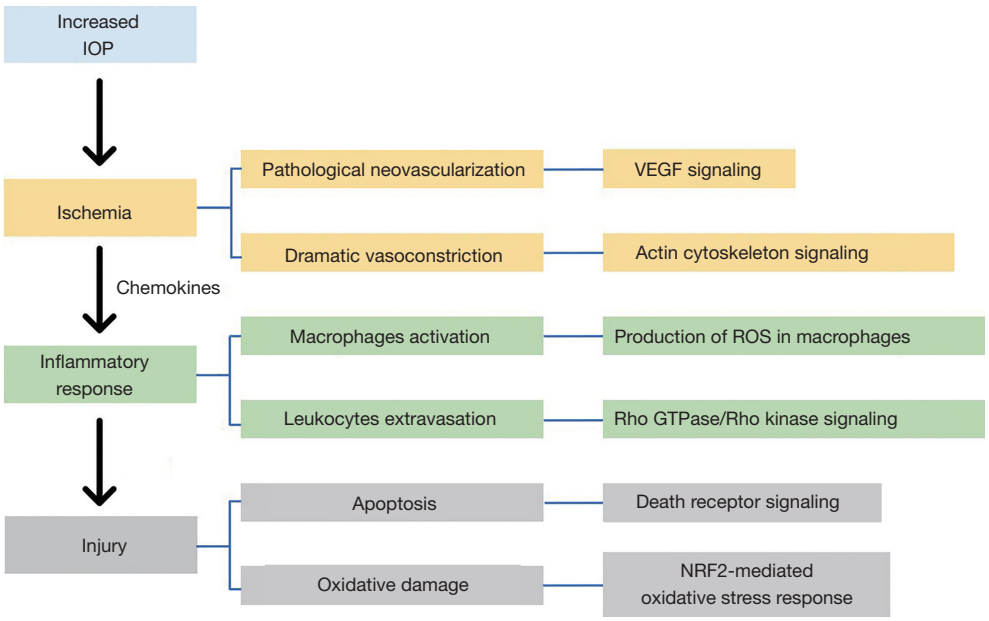

Figure 6 The potential mechanism of VF loss in AACG. The major functions and pathways are shown. VF, visual field; AACG, acute angle-closure glaucoma; IOP, intraocular pressure.

validated proteins, PTGDS showed the best results, with 100% sensitivity and specificity. A previous study reported that it could catalyze the conversion of PGH2 to PGD2. Previously, PGD2 was found to maintain normal cerebral blood flow and contribute to recovery from hypoxia from hypoxic–ischemic injury in the mouse brain (55), and it was also found to modulate immune and inflammatory responses and induce apoptosis and neuroprotection (56). Another study found that PTGDS protects against oxidative stress-mediated neurodegenerative diseases (57). In this study, the IPA functional analysis indicated that ocular hemodynamic changes and oxidative damage–related pathways, such as occlusion in blood vessels, vasoconstriction, and production of NO and ROS, were upregulated. Therefore, the upregulation of PTGDS in the late stage might play a protective role during AACG to improve ocular blood perfusion and promote ROS scavenging. Therefore, it has potential for use as an objective biomarker of VF loss, but this needs to be confirmed by large-scale clonal validation.

Conclusions

In this study, we used a proteomic method to investigate the process of VF loss during AACG. Our study reported the proteomic difference between 2 stages of pathogenesis. Functional analysis showed that the inflammatory response, ocular hemodynamics, and cell apoptosis were closely related to the observed pathological changes. Although the cross-talk between AH proteins and optic nerve behavior is still unclear, our findings may be helpful in further proteomic research of VF loss in AACG. The results of our study indicated that AH could reflect changes in different stages of VF loss and that PTGDS has potential as an objective biomarker of VF loss.

For future work, the following issues should be addressed. First, the samples in this study were from a single center, and thus a large-scale analysis including different glaucoma and control groups (cataracts) from multiple centers should be used to validate the conclusions. Second, the present study did not evaluate the impact factors of AH proteome; therefore, related factors, including age, gender, BAB, and others should be comprehensively analyzed. Third, for examining the role of proteins in VF loss, molecular biology and related animal models should be used, which may help clarify the possible mechanism of VF loss and improve our understanding of it.

Acknowledgments

Funding: This work was supported by National Key Research and Development Program of China (No. 2016YFC1306300 and 2018YFC0910202), the National

Natural Science Foundation of China (No. 30970650, 31200614, 31400669, 81371515, 81170665, and 81560121), the National Natural Science Foundation of China Youth Science Foundation Project (No. 81700857), the Beijing Natural Science Foundation (No. 7172076), Beijing Medical Research (No. 2018-7), the Beijing Cooperative Construction Project (No. 110651103), Beijing Normal University (No. 11100704), Peking Union Medical College Hospital (No. 2016-2.27), the CAMS Innovation Fund for Medical Sciences (No. 2017-I2M-1-009 and 2018-I2M-1-001), the Jilin Science and Technology Office (No. 20190201051JC), and the Biologic Medicine Information Center of China, National Scientific Data Sharing Platform for Population and Health.

Footnote

Reporting Checklist: The authors have completed the MDAR reporting checklist. Available at https://dx.doi.org/10.21037/atm-21-457

Data Sharing Statement: Available at https://dx.doi.org/10.21037/atm-21-457

Peer Review File: Available at https://dx.doi.org/10.21037/atm-21-457

Conflicts of Interest: All authors have completed the ICMJE uniform disclosure form (available at https://dx.doi.org/10.21037/atm-21-457). XL was employed by Shanghai AB Sciex Analytical Instrument Trading Co., Ltd. The other authors have no conflicts of interest to declare.

Ethical Statement: The authors are accountable for all aspects of the work in ensuring that questions related to the accuracy or integrity of any part of the work are appropriately investigated and resolved. All volunteers were given a verbal explanation of the study before enrolment, and each participant signed an informed consent form. The consent procedure and the research protocol for this study were approved by the Ethics Committee for Human and Animal Research in Peking Union Medical College (047-2019). The study methodologies conformed to the Declaration of Helsinki (as revised in 2013).

References

1. Andreatta W, Elaroud I, Nightingale P, et al. Long-term outcomes after acute primary angle closure in a White Caucasian population. BMC Ophthalmol 2015;15:108.
2. Pohl H, Tarnutzer AA. Acute Angle-Closure Glaucoma. N Engl J Med 2018;378:e14.
3. Xie M, Fan N, Tian X, et al. Optic nerve damage and its mechanism in acute angle-closure glaucoma. International Review of Ophthalmology 2015;39:247-52.
4. Flores-Sánchez BC, Tatham AJ. Acute angle closure glaucoma. Br J Hosp Med (Lond) 2019;80:C174-9.
5. Mukai R, Park DH, Okunuki Y, et al. Mouse model of ocular hypertension with retinal ganglion cell degeneration. PLoS One 2019;14:e0208713.
6. Quigley HA. Glaucoma. Lancet 2011;377:1367-77.
7. Marjanović I, Martinez A, Marjanović M, et al. Changes in the retrobulbar arterial circulation after decrease of the elevated intraocular pressure in men and women with primary open angle glaucoma. Srp Arh Celok Lek 2013;141:728-31.
8. Fick CM, Dubielzig RR. Short posterior ciliary artery anatomy in normal and acutely glaucomatous dogs. Vet Ophthalmol 2016;19:43-9.
9. Lu DW, Chen YH, Chang CJ, et al. Nitric oxide levels in the aqueous humor vary in different ocular hypertension experimental models. Kaohsiung J Med Sci 2014;30:593-8.
10. Sucher NJ, Lipton SA, Dreyer EB. Molecular basis of glutamate toxicity in retinal ganglion cells. Vision Res 1997;37:3483-93.
11. Lusardi TA, Wolf JA, Putt ME, et al. Effect of acute calcium influx after mechanical stretch injury in vitro on the viability of hippocampal neurons. J Neurotrauma 2004;21:61-72.
12. Morrison JC, Johnson EC, Cepurna W, et al. Understanding mechanisms of pressure-induced optic nerve damage. Prog Retin Eye Res 2005;24:217-40.
13. Grus FH, Joachim SC, Pfeiffer N. Proteomics in ocular fluids. Proteomics Clin Appl 2007;1:876-88.
14. Funke S, Perumal N, Bell K, et al. The potential impact of recent insights into proteomic changes associated with

glaucoma. Expert Rev Proteomics 2017;14:311-34.
15. Youngblood H, Robinson R, Sharma A, et al. Proteomic Biomarkers of Retinal Inflammation in Diabetic Retinopathy. Int J Mol Sci 2019;20:4755.
16. Kliuchnikova AA, Samokhina NI, Ilina IY, et al. Human aqueous humor proteome in cataract, glaucoma, and pseudoexfoliation syndrome. Proteomics 2016;16:1938-46.
17. Klenkler B, Sheardown H. Growth factors in the anterior segment: role in tissue maintenance, wound healing and ocular pathology. Exp Eye Res 2004;79:677-88.
18. Vesaluoma M, Mertaniemi P, Mannonen S, et al. Cellular and plasma fibronectin in the aqueous humour of primary open-angle glaucoma, exfoliative glaucoma and cataract patients. Eye (Lond) 1998;12 (Pt 5):886-90.
19. Schlötzer-Schrehardt U, Lommatzsch J, Küchle M, et al. Matrix metalloproteinases and their inhibitors in aqueous humor of patients with pseudoexfoliation syndrome/ glaucoma and primary open-angle glaucoma. Invest Ophthalmol Vis Sci 2003;44:1117-25.
20. Aggarwala KRG. Ocular Accommodation, Intraocular Pressure, Development of Myopia and Glaucoma: Role of Ciliary Muscle, Choroid and Metabolism. Med Hypothesis Discov Innov Ophthalmol 2020;9:66-70.
21. Croft MA, Lütjen-Drecoll E, Kaufman PL. Age-related posterior ciliary muscle restriction - A link between trabecular meshwork and optic nerve head pathophysiology. Exp Eye Res 2017;158:187-9.
22. Izzotti A, Longobardi M, Cartiglia C, et al. Proteome alterations in primary open angle glaucoma aqueous humor. J Proteome Res 2010;9:4831-8.
23. Kaeslin MA, Killer HE, Fuhrer CA, et al. Changes to the Aqueous Humor Proteome during Glaucoma. PLoS One 2016;11:e0165314.
24. Wang LM, Dong LJ, Liu X, et al. Proteomic analysis of aqueous humor in acute primary angle-closure glaucoma. Zhonghua Yan Ke Za Zhi 2019;55:687-94.
25. Hirasawa K, Shoji N, Morita T, et al. A modified glaucoma staging system based on visual field index. Graefes Arch Clin Exp Ophthalmol 2013;251:2747-52.
26. Yu M, Xie F, Liu X, et al. Proteomic Study of Aqueous Humor and Its Application in the Treatment of Neovascular Glaucoma. Front Mol Biosci 2020;7:587677.
27. Schneider M, Fuchshofer R. The role of astrocytes in optic nerve head fibrosis in glaucoma. Exp Eye Res 2016;142:49-55.
28. Tektas OY, Lütjen-Drecoll E, Scholz M. Qualitative and quantitative morphologic changes in the vasculature and extracellular matrix of the prelaminar optic nerve head in eyes with POAG. Invest Ophthalmol Vis Sci 2010;51:5083-91.
29. Russo R, Varano GP, Adornetto A, et al. Retinal ganglion cell death in glaucoma: Exploring the role of neuroinflammation. Eur J Pharmacol 2016;787:134-42.
30. Oka T, Tamada Y, Nakajima E, et al. Presence of calpain-induced proteolysis in retinal degeneration and dysfunction in a rat model of acute ocular hypertension. J Neurosci Res 2006;83:1342-51.
31. Määttä M, Tervahartiala T, Harju M, et al. Matrix metalloproteinases and their tissue inhibitors in aqueous humor of patients with primary open-angle glaucoma, exfoliation syndrome, and exfoliation glaucoma. J Glaucoma 2005;14:64-9.
32. Ozcan AA, Ozdemir N, Canataroglu A. The aqueous levels of TGF-beta2 in patients with glaucoma. Int Ophthalmol 2004;25:19-22.
33. Funding M, Vorum H, Honoré B, et al. Proteomic analysis of aqueous humour from patients with acute corneal rejection. Acta Ophthalmol Scand 2005;83:31-9.
34. Caprioli J, Coleman AL; Blood Flow in Glaucoma Discussion. Blood pressure, perfusion pressure, and glaucoma. Am J Ophthalmol 2010;149:704-12.
35. Harris A, Guidoboni G, Arciero JC, et al. Ocular hemodynamics and glaucoma: the role of mathematical modeling. Eur J Ophthalmol 2013;23:139-46.
36. Cabral T, Mello LGM, Lima LH, et al. Retinal and choroidal angiogenesis: a review of new targets. Int J Retina Vitreous 2017;3:31.
37. Park K, Jin J, Hu Y, et al. Overexpression of pigment epithelium-derived factor inhibits retinal inflammation and neovascularization. Am J Pathol 2011;178:688-98.
38. Iliff JJ, Alkayed NJ, Gloshani KJ, et al. Cocaine- and amphetamine-regulated transcript (CART) peptide: a vasoactive role in the cerebral circulation. J Cereb Blood Flow Metab 2005;25:1376-85.
39. Xu Y, Zhang W, Klaus J, et al. Role of cocaine- and amphetamine-regulated transcript in estradiol-mediated neuroprotection. Proc Natl Acad Sci U S A 2006;103:14489-94.
40. Mac Nair CE, Nickells RW. Neuroinflammation in Glaucoma and Optic Nerve Damage. Prog Mol Biol Transl Sci 2015;134:343-63.
41. Neufeld AH, Kawai Si, Das S, et al. Loss of retinal ganglion cells following retinal ischemia: the role of inducible nitric oxide synthase. Exp Eye Res 2002;75:521-8.
42. Guo M, Yan H. Research progress in the mechanism and treatment of retinal ischemia reperfusion injury. Chinese

Journal of Ocular Fundus Diseases 2020;36:483-8.
43. Hirooka K, Miyamoto O, Jinming P, et al. Neuroprotective effects of D-allose against retinal ischemia-reperfusion injury. Invest Ophthalmol Vis Sci 2006;47:1653-7.
44. Millán J, Ridley AJ. Rho GTPases and leucocyte-induced endothelial remodelling. Biochem J 2005;385:329-37.
45. Wittchen ES, van Buul JD, Burridge K, et al. Trading spaces: Rap, Rac, and Rho as architects of transendothelial migration. Curr Opin Hematol 2005;12:14-21.
46. Zhu YJ, Jin M. Advances in the mechanism of retina ischemia-reperfusion injury. Chinese Journal of Pathophysiology 2007;23:195-200.
47. Kaur C, Foulds WS, Ling EA. Hypoxia-ischemia and retinal ganglion cell damage. Clin Ophthalmol 2008;2:879-89.
48. Kortuem K, Geiger LK, Levin LA. Differential susceptibility of retinal ganglion cells to reactive oxygen species. Invest Ophthalmol Vis Sci 2000;41:3176-82.
49. Levkovitch-Verbin H, Harris-Cerruti C, Groner Y, et al. RGC death in mice after optic nerve crush injury: oxidative stress and neuroprotection. Invest Ophthalmol Vis Sci 2000;41:4169-74.
50. Lieven CJ, Vrabec JP, Levin LA. The effects of oxidative stress on mitochondrial transmembrane potential in retinal ganglion cells. Antioxid Redox Signal 2003;5:641-6.
51. He Y, Liu JN, Zhang JJ, et al. Involvement of microRNA-181a and Bim in a rat model of retinal ischemia-reperfusion injury. Int J Ophthalmol 2016;9:33-40.
52. Chen L, Shi JM. Research advances on mechanism of apoptosis in retinal ganglion cells in glaucoma. Recent Advances in Ophthalmology 2013;33:384-8.
53. Zhou X, Meng Q, Xu X, et al. Bex2 regulates cell proliferation and apoptosis in malignant glioma cells via the c-Jun NH2-terminal kinase pathway. Biochem Biophys Res Commun 2012;427:574-80.
54. Giampietro C, Taddei A, Corada M, et al. Overlapping and divergent signaling pathways of N-cadherin and VE-cadherin in endothelial cells. Blood 2012;119:2159-70.
55. Taniguchi H, Mohri I, Okabe-Arahori H, et al. Prostaglandin D2 protects neonatal mouse brain from hypoxic ischemic injury. J Neurosci 2007;27:4303-12.
56. Wei Q, Zhang T, Fan J, et al. Pathological myopia-induced antioxidative proteins in the vitreous humor. Ann Transl Med 2020;8:193.
57. Fukuhara A, Yamada M, Fujimori K, et al. Lipocalin-type prostaglandin D synthase protects against oxidative stress-induced neuronal cell death. Biochem J 2012;443:75-84.

(English Language Editors: J. Jones and J. Gray)

Cite this article as: Xu J, Zhao L, Liu X, Sun H, Liu X, Guo Z, Wang Y, Sun W. Aqueous humor proteomic analysis of acute angle-closure glaucoma with visual field loss. Ann Transl Med 2021;9(21):1611. doi: 10.21037/atm-21-457

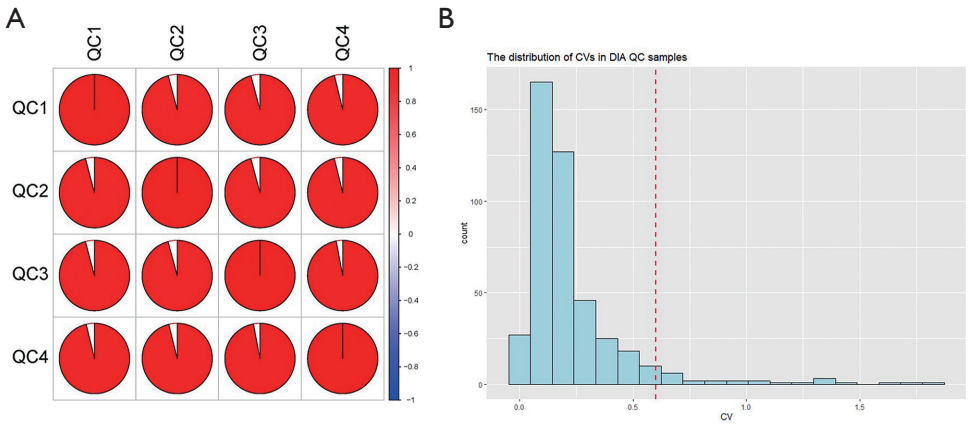

Figure S1 Correlation and CVs of QC samples in DIA. (A) Correlation analysis results. (B) CV distribution. CV, coefficient of variation; QC, quality control; DIA, data-independent acquisition.

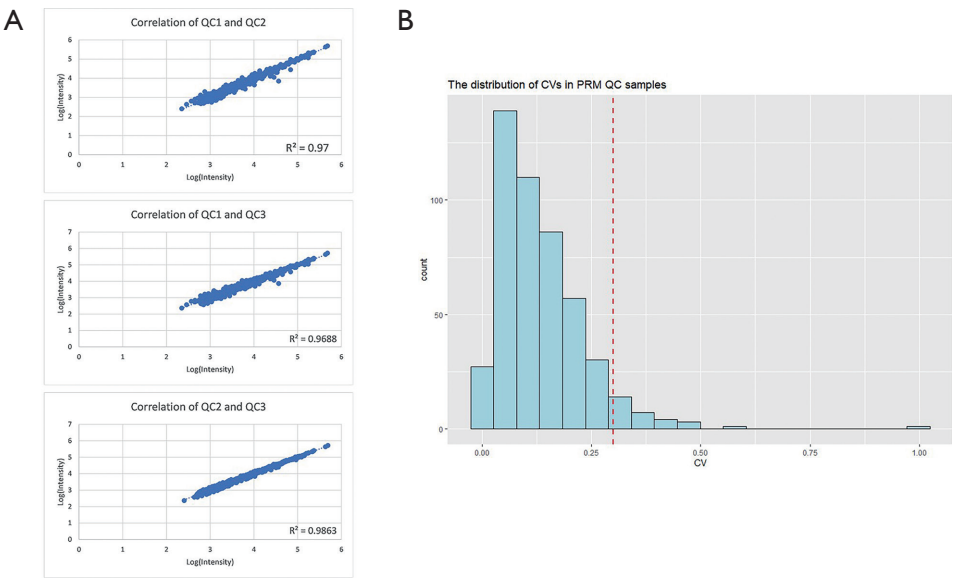

Figure S2 Correlation and CVs of QC samples in PRM. (A) Correlation analysis results. (B) CV distribution. CV, coefficient of variation; QC, quality control; PRM, parallel reaction monitoring.

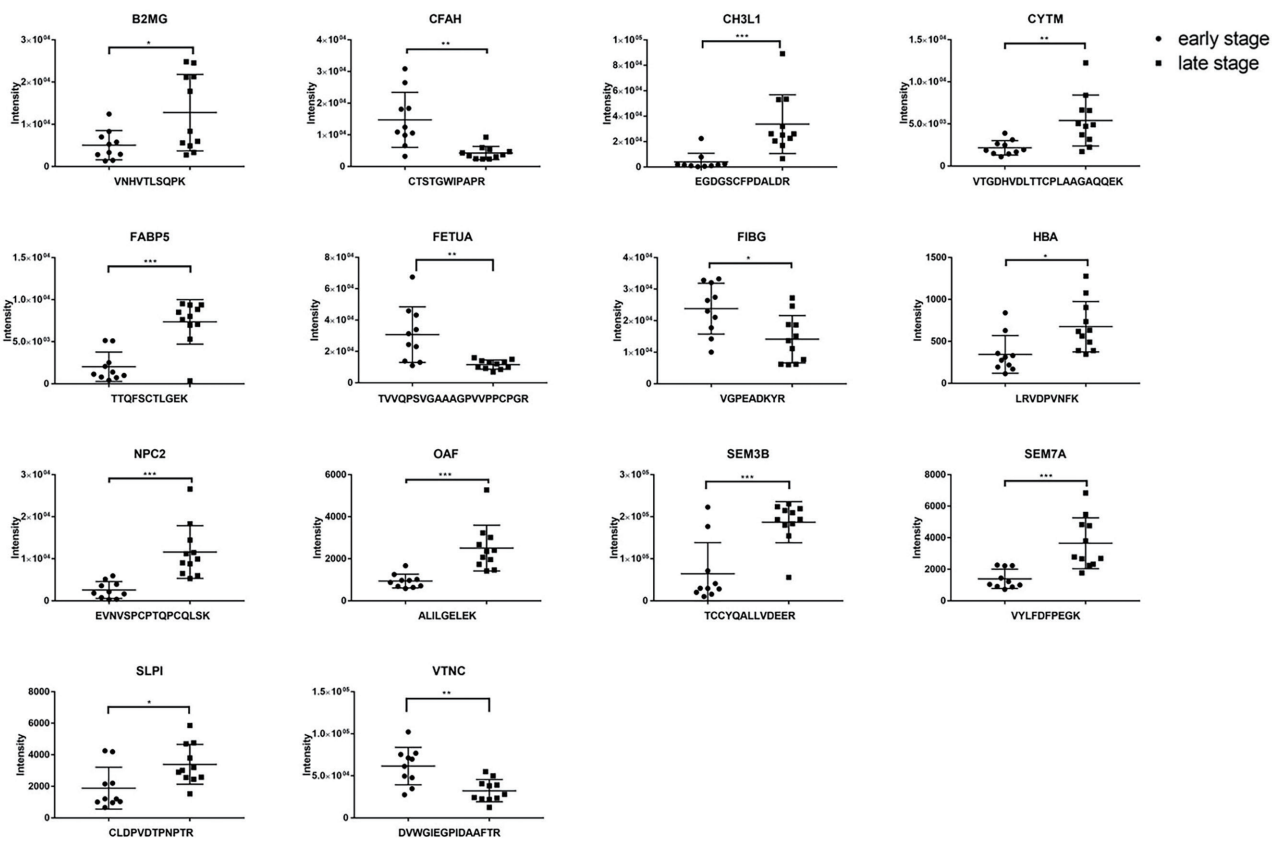

Figure S3 The validated proteins by PRM method. The asterisks indicate the level of significance. *, P<0.05; **, P<0.01; ***, P<0.001. PRM, parallel reaction monitoring.

https://dx.doi.org/10.21037/atm-21-457

Table S1 The clinical information of participants

Number	Gender	Age	Diagnosis	VFI	IOP	Group
H1	Female	70	AACG	92	8	Experiment
H2	Female	67	AACG	94	25	Experiment
H3	Female	59	AACG	95	10	Experiment
H4	Female	64	AACG	97	17	Experiment
H5	Female	64	AACG	85	16	Experiment
H6	Female	73	AACG	98	13	Experiment
H7	Female	68	AACG	95	42	Experiment
H8	Female	64	AACG	97	15	Experiment
H9	Male	70	AACG	88	8	Experiment
H10	Female	72	AACG	95	8	Experiment
H11	Female	70	AACG	97	22	Experiment
H12	Female	63	AACG	99	36	Experiment
H13	Female	56	AACG	91	34	Experiment
H14	Female	63	AACG	98	35	Experiment
H15	Male	70	AACG	82	15	Experiment
H16	Female	67	AACG	86	26	Validation
H17	Female	59	AACG	94	48	Validation
H18	Female	62	AACG	88	10	Validation
H19	Female	51	AACG	95	13	Validation
H20	Female	62	AACG	92	T+2	Validation
H21	Male	72	AACG	86	44	Validation
H22	Female	57	AACG	98	50	Validation
H23	Female	63	AACG	85	23	Validation
H24	Female	58	AACG	94	15	Validation
H25	Female	61	AACG	98	35	Validation
L1	Female	80	AACG	0	25	Experiment
L2	Female	70	AACG	0.59	14	Experiment
L3	Female	79	AACG	18	T+2	Experiment
L4	Female	61	AACG	0	32	Experiment
L5	Female	81	AACG	20	50	Experiment
L6	Female	75	AACG	0	30	Experiment
L7	Female	78	AACG	5	T+2	Experiment
L8	Female	50	AACG	23	15	Experiment
L9	Male	65	AACG	0	T+2	Experiment
L10	Female	69	AACG	21	16	Experiment
L11	Female	76	AACG	24	40	Experiment
L12	Male	68	AACG	8	17	Experiment
L13	Female	66	AACG	27	45	Experiment
L14	Female	60	AACG	36	18	Experiment
L15	Female	56	AACG	35	55	Experiment
L16	Female	68	AACG	8	17	Experiment
L17	Female	65	AACG	0	T+2	Validation
L18	Female	65	AACG	0	T+2	Validation
L19	Female	72	AACG	4	20	Validation
L20	Female	66	AACG	0	35	Validation
L21	Female	60	AACG	0	14	Validation
L22	Female	60	AACG	34	16	Validation
L23	Male	70	AACG	5	7	Validation
L24	Female	80	AACG	0	T+3	Validation
L25	Female	66	AACG	6	56	Validation
L26	Female	73	AACG	9		Validation
L27	Female	86	AACG	0		Validation

VFI, visual field index; IOP, intraocular pressure.

https://dx.doi.org/10.21037/atm-21-457

https://dx.doi.org/10.21037/atm-21-457

Table S2 The AH proteome results of PRM

Peptide	Protein	Protein name	L17	L18	L19	L20	L21	L22	L23	L24	L25	L26	L27	H16	H17	H18	H19	H20	H21	H22	H23	H24	H25	FC (late/early)
TVVQPSVGAAAGPVVPPCPGR	P02765	FETUA_HUMAN	12124.94	9213.218	9968.591	9915.957	6868.24	8568.323	15049.73	13034.23	16021.53	14026.64	13359.04	43251.94778	11026.6316	13099.46	33978.56114	45922.31	24401.05664	67495	23128.12	31351.4713	13928.37261	0.378761
CTSTGWIPAPR	P08603	CFAH_HUMAN	3415.899	4713.334	3708.854	2397.625	4350.448	2367.399	9279.81	3082.294	2467.996	5422.084	5993.191	18373.2161	6588.335086	10585.52	10902.07905	26469.79	12440.91026	30885.75	18115.22	9867.886813	3245.500093	0.290953
DVWGIEGPIDAAFTR	P04004	VTNC_HUMAN	40720.89	50009.97	22502.56	23560.62	12523.5	21841.91	55005.28	24319.09	39168.69	28082.59	38168.68	75416.09709	49626.20756	71267.7	76983.37891	102336.1	34855.18134	61421.24	69904.45	47870.45543	27519.02023	0.524221
VGPEADKYR	P02679	FIBG_HUMAN	7702.341	6223.975	18694.77	6203.559	13672.5	11144.31	18771.17	24651.25	6048.99	27234.6	15141.83	17786.1391	21090.45621	26452.72	27445.40184	32853.46	23057.14837	10062.87	32085.92	33279.57419	14251.25255	0.593015
YGQVPMCDAGEQCAVR	Q16568	CART_HUMAN	659.0818	631.3973	801.8015	366.9468	275.7723	987.57	456.228	291.9171	194.1919	1235.998	541.8668	331.1716379	401.9273599	275.2125	379.5196277	271.2662	534.1378195	137.9973	141.3171	133.5766911	452.3102616	1.915052
CLDPVDTPNPTR	P03973	SLPI_HUMAN	5861.852	4760.924	2903.151	2583.257	3019.277	4705.725	2448.396	2566.408	1528.842	3802.334	3194.191	1012.51069	1033.37161	2206.057	4196.936023	1212.42	1204.100394	969.3744	2153.734	4256.570897	665.7079235	1.796683
CECFPGLAVGLDGR	P35555	FBN1_HUMAN	1723.011	2383.289	1194.202	2137.645	1417.665	3236.83	1923.03	1413.419	1467.206	2370.196	1409.739	1081.683986	608.528935	955.2562	867.0290324	1124.545	1050.351551	1107.372	598.4739	445.255637	1088.791984	2.105519
ELLDTVTAPQK	P36955	PEDF_HUMAN	201910.4	243733.5	289058.8	174989	203839	175134.9	58290.37	107439.7	113899.2	254922.7	95019.31	3671.202476	99572.13832	56575.42	27181.42682	5774.277	24256.86732	2309.758	10777.55	27610.59402	82924.47578	5.119133
VTGDHVDLTTCPLAAGAQQEK	Q15828	CYTM_HUMAN	4719.604	6609.882	5040.452	6659.484	3713.891	12257.87	4907.556	1722.619	2240.813	8402.551	3185.889	1490.272371	2639.626109	1681.411	3128.148313	1449.619	3905.061284	1108.503	2499.304	1937.591948	1863.982186	2.490615
TCCYQALLVDEER	Q13214	SEM3B_HUMAN	214889	193081.8	183688.3	219089.1	180246.6	223847	55831.62	154528.6	209745.1	230554.5	194141.1	15972.58014	222757.2362	71617.35	29920.27866	41141.73	20426.68889	10324.91	29580.83	28454.75491	176892.7445	2.893577
ESAEVEEIVFPR	P19022	CADH2_HUMAN	3575.549	4548.888	4717.725	3173.97	3176.861	9988.763	3147.642	1583.408	2250.888	5404.495	1926.699	689.9409124	2211.873553	1359.724	1758.055793	648.2371	2296.274817	607.4143	998.0999	1307.664711	2089.905363	2.830978
TTQFSCTLGEK	Q01469	FABP5_HUMAN	7072.779	6968.93	8861.063	7635.611	8519.023	9371.762	5309.964	351.3422	9528.246	9399.238	8022.286	415.03978	5145.033942	2524.839	1393.201444	2063.788	731.7010995	999.9148	806.2022	1145.620856	5101.131935	3.624483
EGDGSCFPDALDR	P36222	CH3L1_HUMAN	26092.77	32058.49	53008.92	20547.1	26248.42	89167.88	6658.776	22653.52	16955.94	53464.53	25109.63	262.715163	22462.82899	2403.208	1845.603061	1020.114	1045.571794	599.1194	1594.257	1553.650202	7985.711635	8.293545
AQGFTEDTIVFLPQTDK	P41222	PTGDS_HUMAN	398619.2	414132.1	411951.8	476248.2	361390.8	1205236	295046.2	260084.6	299425.6	819958.4	452854.5	15739.25466	196570.8503	161441.9	94533.71747	25042.46	63881.8476	4960.362	43503.26	54713.88858	255095.565	5.357278
ALILGELEK	Q86UD1	OAF_HUMAN	2073.638	3232.848	5278.735	2348.699	2414.711	2680.283	1738.8	1465.978	1422.56	3015.644	1964.336	694.9586645	1255.613798	1673.423	875.4726775	587.1067	635.707651	978.8004	972.2304	714.9637646	1022.453145	2.669702
LRVDPVNFK	P69905	HBA_HUMAN	632.5739	904.2175	563.7971	617.8137	346.2704	735.1397	491.832	1278.232	389.3716	390.147	1078.199	218.6306268	356.8241992	841.2499	629.7181645	114.6195	311.8791295	275.9946	330.8981	193.7956912	169.7903136	1.960957
VYLFDFPEGK	O75326	SEM7A_HUMAN	4768.403	3802.991	4833.383	2692.862	2668.563	6845.152	1778.544	2321.605	2248.32	5485.509	2786.269	732.2333943	2271.162385	2238.008	1006.571378	884.4807	1220.43123	916.2115	1448.693	1042.336147	2223.510855	2.615498
DFEPSLGPVCPFR	P07585	PGS2_HUMAN	5375.071	9188.245	3476.703	3308.997	2716.253	4704.802	919.494	1669.349	3089.489	7972.963	3807.459	1144.764298	2549.783523	1783.798	1564.296358	822.0767	856.3730887	1175.993	1222.431	1674.088202	1585.63741	2.922699
VVQCSDLGLDK	P07585	PGS2_HUMAN	2005.561	3900.999	1582.144	1122.665	1188.694	1465.665	1494.954	1693.498	1052.746	3177.673	1266.939	874.1640963	1291.623579	1193.072	1065.676894	1485.278	1311.246608	998.4066	886.8996	1072.628129	1188.532195	1.595576
EVNVSPCPTQPCQLSK	P61916	NPC2_HUMAN	9927.194	9032.751	18341.66	8811.04	11490.02	26624.24	6505.596	5305.883	6019.16	14451.96	11224.23	393.1767173	5957.618306	3936.846	3599.21483	775.5922	1668.533427	301.6334	1838.28	2164.234367	5173.501577	4.499331
VNHVTLSQPK	P61769	B2MG_HUMAN	5600.99	8359.418	24844.7	4881.591	17840.48	21275.21	24538.61	2769.069	3334.056	21131.9	5959.982	1336.155699	7020.452465	8306.481	5276.389391	2907.197	2842.362028	1487.807	12440.15	5791.24299	3337.353869	2.517657
ISPDLCGR	P35555	FBN1_HUMAN	2941.168	4538.522	1140.414	2530.494	2211.806	2971.478	2510.496	1759.789	1666.139	3065.212	2054.002	380.990748	1364.370613	1735.146	914.135684	894.3507	1030.834211	322.7478	797.3216	669.34331	1607.904992	2.562436
TSLEDFYLDEER	P36955	PEDF_HUMAN	105180.2	132280.6	194813	112659.1	127399.7	268538.7	116425.1	107082.4	85220.83	165027.4	84852.8	13672.29921	56248.73375	78598.96	62534.52451	10250.81	38063.59307	12833.37	26081.49	51157.31794	80640.65689	3.169545
LQSLFDSPDFSK	P36955	PEDF_HUMAN	169652.7	177032.5	275230.3	171974.8	157009.8	312086	167954	187539.1	124938.3	240977.6	136293.1	47381.55775	113319.509	189776.5	148795.6918	39006.3	124288.0154	16911.45	90991.19	137399.6852	153110.9668	1.817091
KTSLEDFYLDEER	P36955	PEDF_HUMAN	20035.12	22612.03	53048.49	28493.3	31005.27	41912.19	37901.29	28555.32	23570.12	29529.12	20364.56	4401.285405	9505.491128	28732.12	23232.46733	4333.892	19466.35609	2815.371	10453.99	17093.4369	17318.61199	2.230661

AH, aqueous humor; PRM, parallel reaction monitoring.